Journal of Materials Chemistry C

ROYAL SOCIETY OF CHEMISTRY

PAPER

View Article Online
View Journal | View Issue

Cite this: J. Mater. Chem. C, 2024, 12, 14613

Improved performance of perovskite solar cells by fine-tuning dibenzofuran-based hole transporting materials†

Xuepeng Liu,[a] Xianfu Zhang,[a] Mingyuan Han,[a] Jianlin Chen,[a] Ghadari Rahim,[b] Yongpeng Liang,[a] Botong Li[a] and Songyuan Dai *[a]

Received 25th July 2024,
Accepted 8th August 2024

DOI: 10.1039/d4tc03167a

rsc.li/materials-c

In perovskite solar cells (PSCs), the properties of hole transporting materials (HTMs) have a significant effect on device performance. Molecular engineering of HTMs has been proved to be an effective way to fine-tune material properties and device performance. In this work, a series of spiro-type HTMs with dibenzofuran units as edge groups were developed by varying the substitution positions. It is noted that a newly-developed molecule (named spiro-4) exhibits more matched energy levels with perovskite, a higher glass transition temperature, higher hole mobility, better film-forming ability, and enhanced hole extraction ability than other positional isomers. When used in devices, spiro-4 delivers an impressive power conversion efficiency of 23.38%, which is obviously higher than other dibenzofuran-based counterparts or commercial spiro-OMeTAD. Most importantly, a spiro-4-based device also showed superior stability. The findings provide a promising way to obtain efficient and stable PSCs.

Introduction

Perovskite solar cells (PSCs) have attracted global attention because of their rapidly improving power conversion efficiency (PCE) and facile device fabrication process. Until now, the recorded PCE of PSC has achieved 26.1%,[1] illustrating huge commercial application potential. In the development of PSCs, the replacement of a liquid electrolyte by solid-state hole transporting materials (HTMs) greatly improved the PCE and stability of the device.[2–4] After that, the device performance was significantly enhanced by using different HTMs. HTMs could extract the photogenerated holes and transport them to the electrode, and they have become an essential component of high-performance PSCs.[5–8] At present, 2,2′,7,7′-tetrakis[*N*,*N*-di(4-methoxyphenyl)amino]-9,9′-spirobifluorene (spiro-OMeTAD) is the most commonly used HTM for PSCs due to its good film-forming ability on a perovskite layer and superior isotropic charge transfer ability, *etc.*[9–11] However, spiro-OMeTAD suffers a mismatched energy level with respect to an efficient perovskite, leading to energy loss.[12–15] The glass transition temperature (T_g) of spiro-OMeTAD is around 122 °C, which would drop to ~50 °C after doping and thus limit the device stability.[16] Developing novel HTMs is an essential way to further improve the performance of PSCs.

Dibenzofuran is a common skeletal unit for optoelectronic materials.[17–19] Compared with the anisole units on spiro-OMeTAD, dibenzofuran shows extended π-conjugation and less electron donor strength, which is beneficial for improving its properties as an HTM. In our previous report, we successfully introduced dibenzofuran units as edge groups to partially replace anisole units on spiro-OMeTAD.[20] In general, the matched energy level, high thermal stability, superior film-forming ability on a perovskite layer, and good hydrophobicity are essential characteristics for ideal HTMs.[12,21–23] In organic molecules, the molecular structures have remarkable effects on the above physicochemical properties, including HTMs. Fig. S1 (ESI†) simply summarizes the reported positional isomerism of molecular HTMs in PSCs. Obviously, positional isomerism has a significant impact on molecular properties and device performance, which can be fine-tuned by molecular engineering.

Herein, we design and prepare a series of spiro-type HTMs with dibenzofuran units as peripheral groups through changing the substitution position of the terminal unit in order to study in depth the structure–activity relationship of the molecules. The molecular structures of the investigated compounds are illustrated in Fig. 1. It should be noted that spiro-4 exhibits a lower HOMO level (−5.29 eV), higher glass transition temperature (163 °C), and better film-forming ability and hydrophobicity, leading to better device performance among the

[a] Beijing Key Laboratory of Novel Thin-Film Solar Cells, School of New Energy, North China Electric Power University, Beijing 102206, China. E-mail: sydai@ncepu.edu.cn
[b] Computational Chemistry Laboratory, Department of Organic and Biochemistry, Faculty of Chemistry, University of Tabriz, Tabriz, 5166616471, Iran

† Electronic supplementary information (ESI) available. See DOI: https://doi.org/10.1039/d4tc03167a

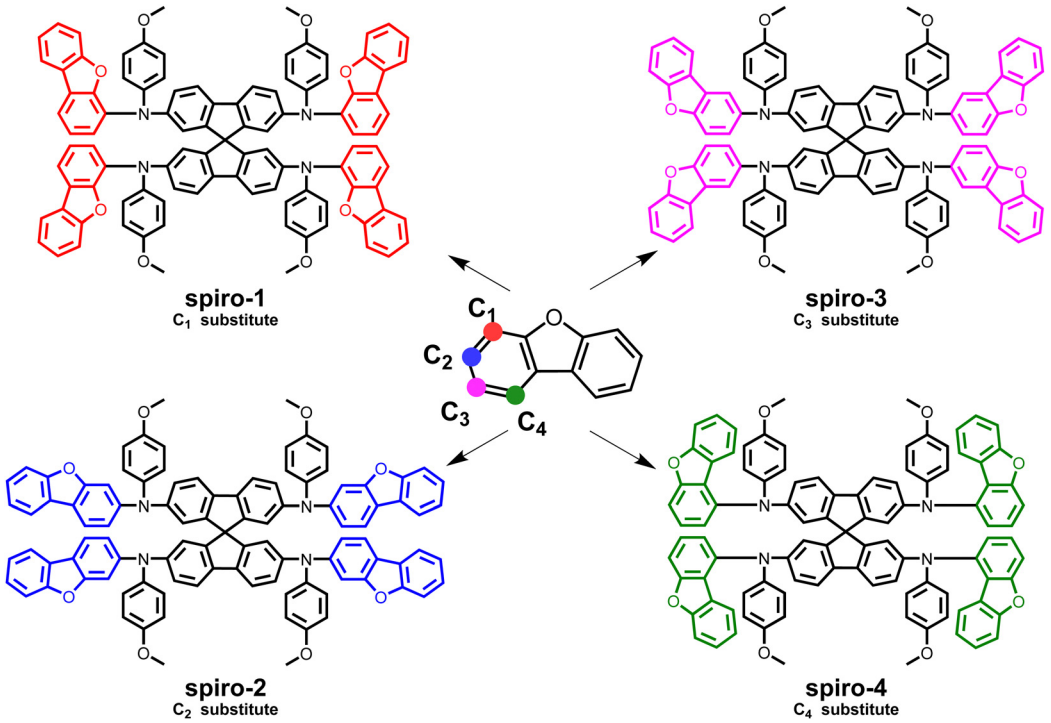

Fig. 1 Molecular structures of the investigated HTMs; the substitution position on dibenzofuran is shown as a colored point.

studied dibenzofuran-based molecules. Importantly, the champion PCE of a spiro-4-based device reaches 23.38%, which is higher than that of spiro-OMeTAD under the same conditions. Moreover, the spiro-4-based device also achieves significantly better device stability than spiro-OMeTAD under moderate or harsh conditions.

Results and discussion

The investigated materials were prepared using a two-step consecutive Buchwald–Hartwig amination reaction. The target molecules were obtained by coupling different available brominated dibenzofuran and N^2,$N^{2\prime}$,N^7,$N^{7\prime}$-tetrakis(4-methoxyphenyl)-9,9′-spirobi[fluorene]-2,2′,7,7′-tetraamine (compound **1** in Scheme S1, ESI†).[24,25] The target materials were determined by NMR spectroscopy and mass spectrometry. Their detailed synthesis process is illustrated in ESI† (Scheme S1).

Fig. 2a and Fig. S2 (ESI†) exhibit the ultraviolet-visible (UV-vis) absorption spectra of the molecules in dichloromethane solution and film states. All the molecules exhibit multiple distinct optical absorption bands from 280 nm to 450 nm. Compared with spiro-OMeTAD, the dibenzofuran-terminated molecules exhibit red- or blue-shifted absorption spectra (Table 1), which probably stem from the various substitution positions changing the electron-withdrawing (electron-donating) and conjugation effect.[13,26] As illustrated in Fig. S2 (ESI†), like spiro-OMeTAD and other organic molecules,[27–29] the absorption onset of all the compounds exhibits a slight bathochromic shift from solution state to film state.

Electrochemical analysis by cyclic voltammetry (CV) was performed, as shown in Fig. 2b. It can obviously be noted that the change in the peripheral group of the molecules from an anisole to a dibenzofuran unit leads to a decreased oxidation potential, which has been observed in many reports (Table S1, ESI†). Interestingly, the oxidation potential reduction of spiro-4 is more significant than that of other molecules. The calculated HOMO level of spiro-4 is −5.29 eV, which is notably deeper-lying than the −5.1 eV of spiro-OMeTAD (similar to the reported value by CV measurements[13,27]). Therefore, spiro-4 may show better air stability and moisture prevention.[27] As far as we know, the difference in HOMO levels (0.19 eV) between spiro-OMeTAD and spiro-4 is also almost the maximum reduction among similar reported spiro-HTMs (Table S1, ESI†). The LUMO levels of the molecules were obtained by adding the HOMO levels and the optical bandgaps (E_g). The energy-level diagram for the perovskite and HTMs in Fig. 2c illustrates that the higher LUMO levels of the molecules could suppress recombination and ensure efficient electron-blocking. The hole mobility of HTM is a key parameter for PSC performance; therefore, space charge-limited current (SCLC) measurements were conducted. As illustrated in Fig. S3 (ESI†), the calculated hole mobilities of spiro-1, spiro-2, spiro-3 and spiro-4 are around 9.2×10^{-4}, 6.15×10^{-3}, 1.46×10^{-3}, and 6.98×10^{-3} $cm^2\ V^{-1}\ s^{-1}$.

To explore the properties of these molecules theoretically, TDDFT calculations were performed, as illustrated Fig. S4 (ESI†). The variation in terminal group of the molecules does not affect the spiro structure, which ensures the isotropic charge transfer of these materials. Compared with spiro-OMeTAD, the HOMO/LUMO distributions of these dibenzofuran-containing

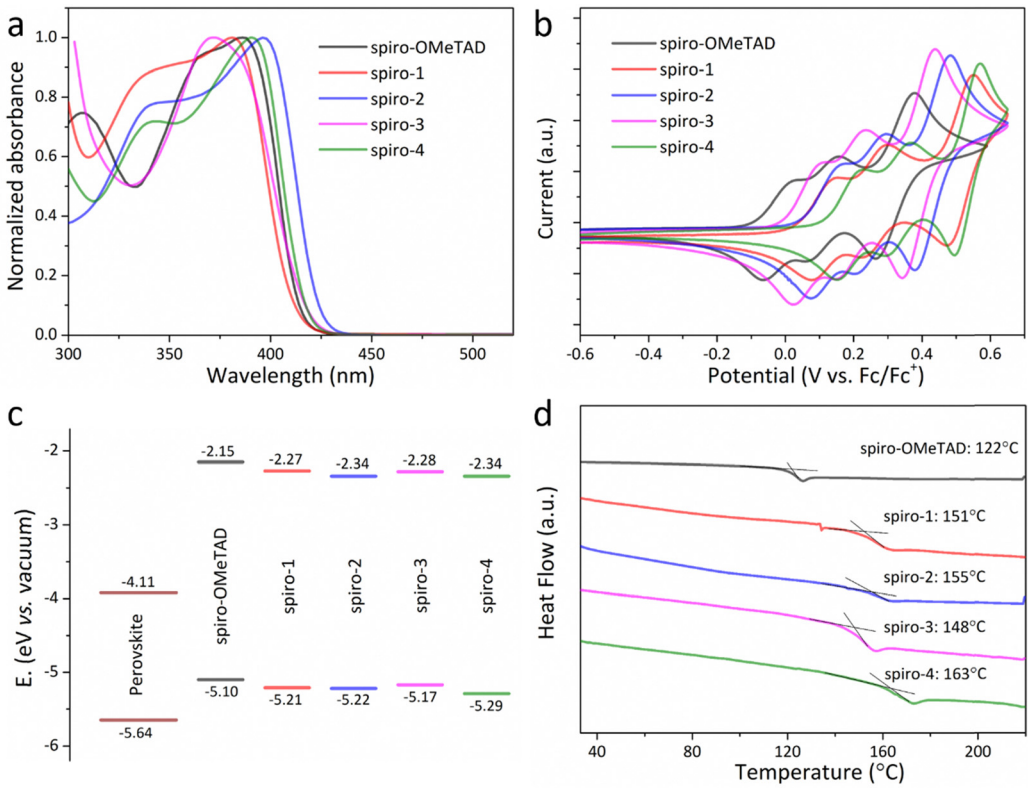

Fig. 2 (a) UV-vis absorption spectra in DCM solution; (b) CV curves; (c) energy-level diagram of the device with studied HTMs; (d) DSC curves.

molecules are more delocalized, consistent with the reported HTM with extended conjugation. Therefore, the HOMO level of these molecules is lower than that of spiro-OMeTAD. Moreover, spiro-4 seems to show most electron delocalization, illustrating its better conjugation. The calculated hole reorganization energies for spiro-OMeTAD, spiro-1, spiro-2, spiro-3, and spiro-4 are 0.162, 0.169, 0.152, 0.161, and 0.146 eV, respectively, illustrating that spiro-4 has a strong driving force for hole transport.[30]

Fig. 2d shows the differential scanning calorimetry (DSC) curves for the investigated materials and spiro-OMeTAD. The replacement of anisole by dibenzofuran could obviously enhance the glass-transition temperature (T_g), similar to reported spiro-based HTMs with extended π-conjugation, which can result from increased molecular weight and reduced molecular symmetry.[24,28,31] Spiro-4 even exhibits a T_g value of 163 °C, which is over 40 °C higher than that of spiro-OMeTAD, thus improving the stability of the overall device. As also illustrated in Table S1 (ESI†), the T_g value of spiro-4 is almost one of the highest values reported for spiro molecules with a similar structure. According to the above results, regulation of the substitution position of a peripheral dibenzofuran unit on the molecular structure has a huge effect on the photophysical, electrochemical, and thermodynamic properties of the molecules. Spiro-4 has the best thermal stability and may show more efficient interfacial hole-transport kinetics, resulting in lower energy loss.[12,13] Time-resolved photoluminescence spectra were performed to study the dynamics of charge migration between the interface of the HTM and the perovskite layer. As shown in Fig. S6 (ESI†), the average decay times for perovskite coated with spiro-1, spiro-2, spiro-3, or spiro-4 are around 8.8, 8.4, 7.7, and 6.6 ns, respectively, illustrating more efficient charge extraction at the perovskite/spiro-4 interface.

To evaluate these molecules as HTMs for PSCs and prove the feasibility of the molecular design in this work, we fabricated a conventional n–i–p PSC with a configuration of fluorine-doped tin oxide substrate/compact TiO_2/mesoporous TiO_2/perovskite layer/HTM/Au; the device configuration is simply illustrated in Fig. 3a. The component of the perovskite in the work is

Table 1 Photophysical, electrochemical and thermal properties of the molecules

HTM	λ_{max} [a] (nm)	λ_{emm} [a,b] (nm)	E_g [c] (eV)	HOMO (eV)	LUMO (eV)	T_g (°C)
spiro-1	381	422	2.94	−5.21	−2.27	151
spiro-2	396	434	2.88	−5.22	−2.34	155
spiro-3	372	429	2.89	−5.17	−2.28	148
spiro-4	391	421	2.95	−5.29	−2.34	163
spiro-OMeTAD	386	428	2.95	−5.10	−2.15	122

[a] Measured in dichloromethane solution. [b] Excited at λ_{max}. [c] Calculated from the onset of the absorption spectra for solid-state film.

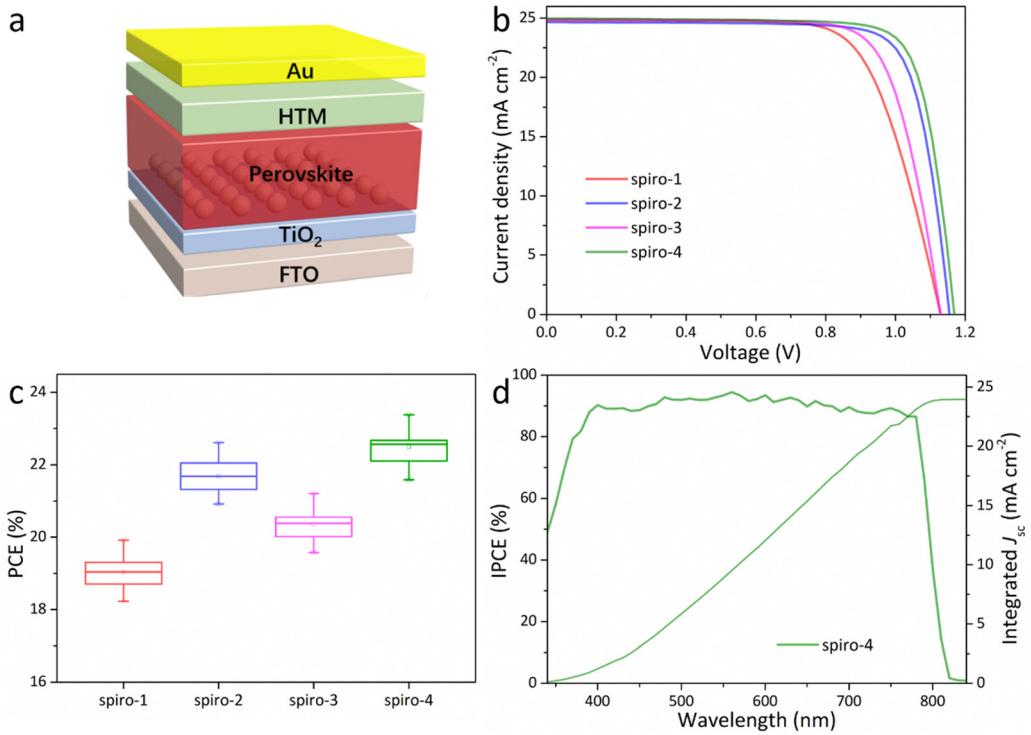

Fig. 3 (a) The structure of the PSC in this work. (b) *J*–*V* curves of the best-performing PSCs with various HTMs measured from reverse scans. (c) Statistical distribution of the PCEs of 16 PSCs with different dibenzofuran-based HTMs. (d) IPCE spectra of the device employing spiro-4.

$Cs_{0.05}FA_{0.95}PbI_3$, and the valence band and the conduction band are −5.64 and −4.11 eV, respectively (Fig. 2c).[29,32] The detailed device fabrication process is described in ESI.† All the HTMs, including spiro-OMeTAD, were doped using conventional 4-*tert*-butylpyridine (TBP), lithium bis(trifluoromethanesulfonyl)-imide, and tris[2-(1 *H*-pyrazol-1-yl)-4-*tert*-butylpyridine]-cobalt(III)-tris[bis-(trifluoromethylsulfonyl)imide]. As with previous reports, the amount of dopants and the amount deposited, and the detailed conditions have been noted in the device fabrication process.[31,33] Cross-sectional scanning electron microscopy of a representative device is exhibited in Fig. S7 (ESI†), where the thickness of the HTM layer is around 120 nm. The film morphology of the HTM on the perovskite layer was analysed by atomic force microscope (AFM) measurements, as shown in Fig. S8a–e (ESI†). The root mean square (RMS) of the bare perovskite layer is around 48 nm, which is greatly reduced after coating with HTMs. The spiro-4-based film exhibits an RMS of 9 nm, which is visibly lower than that of other molecules, illustrating its superior film-forming ability. On the other hand, the molecular kinetic barrier of HTM to water and oxygen is also an important influencing factor for device stability. Therefore, water contact angle measurements were conducted to evaluate the surface wettability of the perovskite film or films coated with different HTMs (doped with the same device fabrication process), as shown in Fig. S8f–j (ESI†). Similar to many spiro-type HTMs with extended π-conjugation groups as end-capping groups,[27,28] dibenzofuran-terminated molecules also exhibit higher contact angles than spiro-OMeTAD. Moreover, spiro-4 exhibits the best hydrophobicity compared to other dibenzofuran counterparts.

Table 2 Photovoltaic parameters of best-performing PSCs with different HTMs (reverse scan)

HTM	V_{oc} (V)	J_{sc} (mA cm^{-2})	FF (%)	PCE (%)	PCE$_{avg}$[a] (%)
spiro-1	1.13	24.84	71	19.92	19.04
spiro-2	1.15	24.68	79	22.61	21.69
spiro-3	1.13	24.91	75	21.21	20.36
spiro-4	1.17	24.98	80	23.38	22.49
spiro-OMeTAD	1.15	24.95	77	22.10	21.71

[a] The average PCE values were derived from 16 devices.

Fig. 3b shows the current density–voltage (*J*–*V*) curves of the best devices among 16 devices, measured under simulated solar illumination (AM 1.5G, 100 mW cm^{-2}). Table 2 lists the photovoltaic parameters of the champion device with different HTMs. It can be noted that spiro-4 presents an obviously higher PCE than other HTMs: the PCE reaches 23.38%, with an open circuit voltage (V_{oc}) of 1.17 V, a short circuit current (J_{sc}) of 24.98 mA cm^{-2}, and a fill factor (FF) of 80%. As displayed in Fig. S9 (ESI†), the steady-state maximum power output of device employing spiro-4 or spiro-OMeTAD was tested for 200 s. The spiro-4-based PSC has a steady-state efficiency of 22.75%, which is also higher than that of the spiro-OMeTAD counterpart (21.5%). Fig. 3c illustrates the PCE distributions of devices employing different HTMs (the average parameters with standard deviation STDEV are summarized in Table S2, ESI†). Narrow PCE distributions illustrate the high reproducibility. The spiro-4 based device exhibits a visibly higher V_{oc}, which could result from the lower-lying HOMO level, leading to minor

energy loss.[13] Not all the devices display a significantly different J_{sc}, and we selected the spiro-4-based device to measure the incident photo-to-current conversion efficiency (IPCE). The integrated photocurrent density is 23.93 mA cm^{-2}, agreeing well with the value obtained from the *J–V* curve (Fig. 3d). As a comparison, the champion spiro-OMeTAD-based device shows a PCE of 22.10% (Fig. S10, ESI†). Moreover, the average PCE of spiro-4-based devices is also higher than that of spiro-OMeTAD. The *J–V* curves of the champion device with spiro-4 or spiro-OMeTAD measured from different scan directions are shown in Fig. S10 (ESI†) and listed in Table S3 (ESI†). Both devices display slight hysteresis behavior; nevertheless, the spiro-4-based device has a higher PCE under different scan directions.

Electrochemical impedance spectroscopy (EIS) measurement of the Nyquist curves of the PSCs with different HTMs were recorded, as exhibited in Fig. S11a (ESI†). It should be noted that the spiro-4-based device shows the highest value of recombination resistance (R_{rec}), which could decrease interfacial charge recombination.[34] On the other hand, Mott–Schottky curves of devices employing different HTMs are shown in Fig. S11b (ESI†). The spiro-4-based device also has higher built-in potential (V_{bi}) than the other molecules (including spiro-OMeTAD); therefore, spiro-4 is beneficial for promoting the driving force for separating charges and preventing charge accumulation at the interface,[35] consistent with the above results.

Stability is a key parameter for commercial PSCs. The devices with different HTMs were investigated to compare their stability. The long-term stability of the unencapsulated PSCs was tracked at room temperature (~30 °C) and with an RH of ~10% in dark conditions for 2400 h. As illustrated in Fig. 4a, the spiro-4-based device maintained 97% of the initial PCE, while the PCE of the spiro-OMeTAD-based PSC decreased by 25% over the same aging time. Moreover, a stability test at high temperature (~60 °C) was conducted to evaluate the practical application of PSCs for 150 h. As illustrated in Fig. 4b, the PCE of the spiro-OMeTAD-based device exhibited a dramatic decrease (~64% of the initial PCE), while the spiro-4-based device retained a over 80% of the PCE over the same aging time. According to the above measurements, the improved stability of spiro-4-based devices can result from higher surface water resistance and T_g value. Moreover, the interaction between HTMs and the perovskite layer is also a possible factor enhancing the efficiency and stability of the device. Theoretically, the lone-pair electrons of O on dibenzofuran could act as a Lewis base and passivate defects through coordination with Pb^{2+} on the surface of the perovskite layer.[36,37] The better exposure of oxygen on the dibenzofuran of spiro-4 may be attributed to the better Pb–O interaction of dibenzofuran than that of methoxy, which may be one of the reasons for the better device performance of spiro-4 than spiro-OMeTAD.

According to the above illustrations and reported results (Fig. S1, ESI†), molecular engineering of HTM by changing the substitution position of the edge groups on the structures is an effective way to develop efficient HTMs. Therefore, we also chose a reported spiro-OMeTAD analogue as a reference (spiro-Naph[27]) and developed a series of molecules by changing the substitution position of methoxy on the naphthalene unit. The molecular structures of the spiro-Naph analogues are illustrated in Fig. S12 (ESI†). Their synthesis process is also illustrated in ESI.† Because the device performance of the molecules determines their possibility of application, we fabricated devices employing these compounds. The detailed device fabrication process is almost the same as for the above dibenzofuran-terminated HTMs (with PEAI passivation, as reported for spiro-Naph). Fig. S13 and Table S4 (ESI†) show the champion device. The reported spiro-Naph still retains the highest PCE among them. The molecular structure has a macroscopic effect on the T_g value; nevertheless, all the T_g values are below 160 °C (Fig. S14a, ESI†). On the other hand, the characteristics of spiro-Naph and spiro-Naph-1 with higher efficiency are exhibited in Fig. S14 (ESI†) and summarized in Table S5 (ESI†). The HOMO levels of spiro-Naph and spiro-Naph-1 are lower than that of spiro-OMeTAD, but the reduction values are lower than spiro-4, which further illustrates the superiority of spiro-4. The above results also indicate that isomeric modification of HTMs is expected to further improve PSC performance.

Conclusions

By varying the substitution position of dibenzofuran on spiro-type HTMs, a series of spiro-type HTMs were developed and

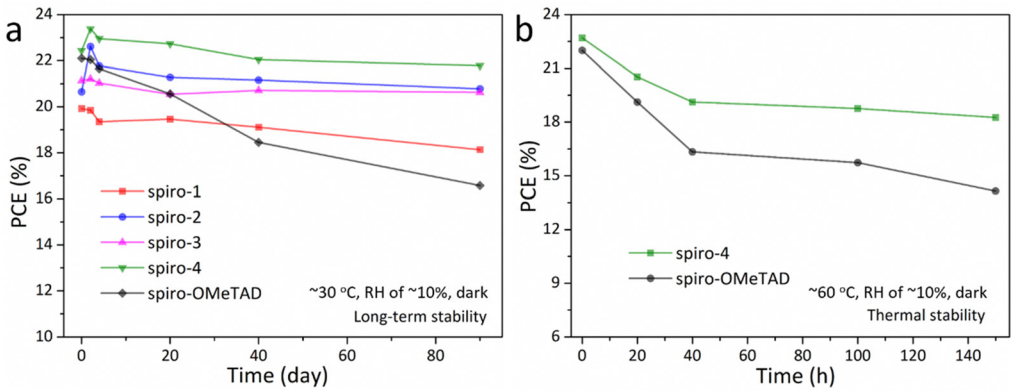

Fig. 4 (a) Long-term stability and (b) thermal stability of devices with different HTMs without encapsulation in air.

investigated. Positional isomerism has a noticeable effect on molecular properties and device performance. Among the investigated molecules, spiro-4 delivers improved photophysics, electrochemistry, thermal stability, *etc.* The champion PSC employing spiro-4 shows a PCE of over 23%, which is slightly higher than that of spiro-OMeTAD. Importantly, the spiro-4-based device also retains superior device stability. Therefore, spiro-4 is a promising HTM candidate, and the results also provide an effective way to improve the performance of a PSC.

Author contributions

X. P. L. designed and prepared the molecules, analysed the data and write the initial draft. X. F. Z. and Y. P. L. carried out the device fabrication. X. F. Z. performed the NMR and MS measurement. M. Y. H. and Y. P. L. performed UV, CV experiments. B. T. L. helped in EIS and M-S measurements. J. L. C. cand B. T. L. carried out the SCLC, TRPL, AFM measurements. G. R. performed TDDFT measurements. S. Y. D. supervised the research and acquired the main funding. All authors contributed to the draft and prepared the final version.

Data availability

The data supporting the findings of this manuscript are available within the article and/or its ESI.†

Conflicts of interest

There are no conflicts to declare.

Acknowledgements

This work was supported by the National Natural Science Foundation of China (61904053, 22279033), the 111 Project (B16016), and the Special Foundation for Carbon Peak Carbon Neutralization Technology Innovation Program of Jiangsu Province (BE2022026).

References

1 NREL Research Cell Record Efficiency Chart, **https://www.nrel.gov/pv/cell-efficiency.html** (accessed 2024-02-28).
2 A. Kojima, K. Teshima, Y. Shirai and T. Miyasaka, *J. Am. Chem. Soc.*, 2009, **131**, 6050–6051.
3 J. H. Im, C. R. Lee, J. W. Lee, S. W. Park and N. G. Park, *Nanoscale*, 2011, **3**, 4088–4093.
4 H. S. Kim, C. R. Lee, J. H. Im, K. B. Lee, T. Moehl, A. Marchioro, S. J. Moon, R. Humphry-Baker, J. H. Yum, J. E. Moser, M. Gratzel and N. G. Park, *Sci. Rep.*, 2012, **2**, 591.
5 X. Yin, Z. Song, Z. Li and W. Tang, *Energy Environ. Sci.*, 2020, **13**, 4057–4086.
6 F. H. Isikgor, S. Zhumagali, L. V. T. Merino, M. D. Bastiani, I. McCulloch and S. D. Wolf, *Nat. Rev. Mater.*, 2023, **8**, 89–108.
7 X. Liu, B. Li, M. Han, X. Zhang, J. Chen and S. Dai, *Acta Chim. Sinica*, 2024, **82**, 348–366.
8 X. Zhang, X. Liu, F. F. Tirani, B. Ding, J. Chen, G. Rahim, M. Han, K. Zhang, Y. Zhou, H. Quan, B. Li, W. Du, K. G. Brooks, S. Dai, Z. Fei, A. M. Asiri, P. J. Dyson, M. K. Nazeeruddin and Y. Ding, *Angew. Chem., Int. Ed.*, 2024, **63**, e202320152.
9 A. Farokhi, H. Shahroosvand, G. Delle Monache, M. Pilkington and M. K. Nazeeruddin, *Chem. Soc. Rev.*, 2022, **51**, 5974–6064.
10 H. Min, D. Lee, J. Kim, G. Kim, K. S. Lee, J. Kim, M. J. Paik, Y. K. Kim, K. S. Kim, M. G. Kim, T. J. Shin and S. I. Seok, *Nature*, 2021, **598**, 444–450.
11 J. Park, J. Kim, H. S. Yun, M. J. Paik, E. Noh, H. J. Mun, M. G. Kim, T. J. Shin and S. I. Seok, *Nature*, 2023, **616**, 724–730.
12 Z. Guo, A. K. Jena, G. M. Kim and T. Miyasaka, *Energy Environ. Sci.*, 2014, **15**, 3171–3222.
13 M. Jeong, I. W. Choi, E. M. Go, Y. Cho, M. Kim, B. Lee, S. Jeong, Y. Jo, H. W. Choi, J. Lee, J. H. Bae, S. K. Kwak, D. S. Kim and C. Yang, *Science*, 2020, **369**, 1615–1620.
14 Y. G. Yao, C. D. Cheng, C. Y. Zhang, H. L. Hu, K. Wang and S. De Wolf, *Adv. Mater.*, 2022, **34**, 31.
15 Y. Zhou, X. Liu, X. Zhang, M. Han, J. Chen, Y. Liang, B. Li, Y. Ding, M. Cai and S. Dai, *Prog. Chem.*, 2024, **36**, 612–613.
16 T. Malinauskas, D. Tomkute-Luksiene, R. Sens, M. Daskeviciene, R. Send, H. Wonneberger, V. Jankauskas, I. Bruder and V. Getautis, *ACS Appl. Mater. Interfaces*, 2015, **7**, 11107–11116.
17 W. J. Zhao, Z. K. He and B. Z. Tang, *Nat. Rev. Mater.*, 2020, **5**, 869–885.
18 C. M. Han, Z. S. Zhang, H. Xu, J. Li, Y. Zhao, P. F. Yan and S. Y. Liu, *Chem. – Eur. J.*, 2013, **19**, 1385–1396.
19 Y. P. Liang, N. Wu, X. F. Zhang, R. Ghadari, X. P. Liu, F. L. Guo and S. Y. Dai, *ChemistrySelect*, 2022, **7**, e202201696.
20 Y. P. Liang, J. L. Chen, X. F. Zhang, M. Y. Han, R. Ghadari, N. Wu, Y. Wang, Y. Zhou, X. P. Liu and S. Y. Dai, *J. Mater. Chem. C*, 2022, **10**, 10988–10994.
21 P. Y. Yan, D. B. Yang, H. Q. Wang, S. C. Yang and Z. Y. Ge, *Energy Environ. Sci.*, 2022, **15**, 3630–3669.
22 D. Meng, J. J. Xue, Y. P. Zhao, E. Zhang, R. Zheng and Y. Yang, *Chem. Rev.*, 2022, **122**, 14954–14986.
23 W. D. Ling, F. Liu, Q. Q. Li and Z. Li, *J. Mater. Chem. A*, 2021, **9**, 18148–18163.
24 N. J. Jeon, H. Na, E. H. Jung, T.-Y. Yang, Y. G. Lee, G. Kim, H.-W. Shin, S. Il Seok, J. Lee and J. Seo, *Nat. Energy*, 2018, **3**, 682–689.
25 X. Zhang, X. Liu, N. Wu, R. Ghadari, M. Han, Y. Wang, Y. Ding, M. Cai, Z. Qu and S. Dai, *J. Energy Chem.*, 2022, **67**, 19–26.
26 N. J. Jeon, H. G. Lee, Y. C. Kim, J. Seo, J. H. Noh, J. Lee and S. I. Seok, *J. Am. Chem. Soc.*, 2014, **136**, 7837–7840.
27 M. Jeong, I. W. Choi, K. Yim, S. Jeong, M. Kim, S. J. Choi, Y. Cho, J.-H. An, H.-B. Kim, Y. Jo, S.-H. Kang, J.-H. Bae, C.-W. Lee, D. S. Kim and C. Yang, *Nat. Photonics*, 2022, **16**, 119–125.
28 X. P. Liu, B. Ding, M. Y. Han, Z. H. Yang, J. L. Chen, P. J. Shi, X. Y. Xue, R. Ghadari, X. F. Zhang, R. Wang, K. Brooks, L. Tao, S. Kinge, S. Y. Dai, J. Sheng, P. J. Dyson, M. K. Nazeeruddin and Y. Ding, *Angew. Chem., Int. Ed.*, 2023, **62**, e202304350.

29 Y. Zhou, X. F. Zhang, M. Y. Han, N. Wu, J. L. Chen, G. Rahim, Y. H. Wu, S. Y. Dai and X. P. Liu, *Sol. Energy Mater. Sol. Cells*, 2023, **257**, 8.
30 M. Cheng, K. Aitola, C. Chen, F. Zhang, P. Liu, K. Sveinbjörnsson, Y. Hua, L. Kloo, G. Boschloo and L. Sun, *Nano Energy*, 2016, **30**, 387–397.
31 Z. H. Deng, M. S. He, Y. Zhang, F. Ullah, K. Ding, J. H. Liang, Z. F. Zhang, H. Xu, Y. K. Qiu, Z. Y. Xie, T. Shan, Z. H. Chen, H. L. Zhong and C. C. Chen, *Chem. Mater.*, 2021, **33**, 285–297.
32 T. Q. Niu, W. Y. Zhu, Y. H. Zhang, Q. F. Xue, X. C. Jiao, Z. J. Wang, Y. M. Xie, P. Li, R. F. Chen, F. Huang, Y. Li, L. Yip and Y. Cao, *Joule*, 2021, **5**, 249–269.
33 M. Y. Han, Y. P. Liang, J. L. Chen, X. F. Zhang, R. Ghadari, X. P. Liu, N. Wu, Y. Wang, Y. Zhou, Y. Ding, M. L. Cai, H. B. Chen and S. Y. Dai, *ChemSusChem*, 2022, **15**, e202201485.
34 J. Chen, X. Zhang, X. Liu, B. Li, M. Han, S. Han, Y. Han, J. Liu, W. Dai, R. Ghadari and S. Dai, *ACS Appl. Mater. Interfaces*, 2024, **16**, 22079–22088.
35 X. Zhang, S. Zhang, X. Liao, B. Ding, G. Rahim, K. Zhao, J. Chen, M. Han, Y. Zhou, P. Shi, K. Zhang, S. Kinge, H. Zhang, R. Wang, K. G. Brooks, S. Dai, X. Liu, Z. Fei, P. J. Dyson, M. K. Nazeeruddin and Y. Ding, *Adv. Funct. Mater.*, 2024, **34**, 2314086.
36 L. G. Xu, D. Wu, W. Lv, Y. Xiang, Y. Liu, Y. Tao, J. Yin, M. Y. Qian, P. Li, L. Q. Zhang, S. F. Chen, O. F. Mohammed, O. M. Bakr, Z. Duan, R. F. Chen and W. Huang, *Adv. Mater.*, 2022, **34**, 9.
37 Z. N. Li, Q. Tan, G. C. Chen, H. Gao, J. F. Wang, X. S. Zhang, J. W. Xiu, W. Chen and Z. B. He, *Nanoscale*, 2023, **15**, 1676–1686.